

Isotropic Diffusion Weighting in Radial Fast Spin-Echo Magnetic Resonance Imaging

Joelle E. Sarlls,¹ Rexford D. Newbould,^{1,2} Maria I. Altbach,³ Arthur F. Gmitro,^{1,3,4} Joachim Seeger,³ and Theodore P. Trouard^{1,3*}

Radial fast spin-echo (radial-FSE) methods enable multishot diffusion-weighted MRI (DWMRI) to be carried out without significant artifacts due to motion and/or susceptibility and can be used to generate DWMRI images with high spatial resolution. In this work, a novel method that allows isotropic diffusion weighting to be obtained in a single radial k -space data set is presented. This is accomplished by altering the direction of diffusion weighting gradients between groups of TR periods, which yield sets of radial lines that possess diffusion weighting sensitive to motion in different directions. By altering the diffusion weighting directions and controlling the view ordering appropriately within the sequence, an effectively isotropic diffusion-weighted image can be obtained within one radial-FSE scan. The order in which radial lines are acquired can also be controlled to yield data sets without significant artifacts due to motion, T_2 decay, and/or diffusion anisotropy. Magn Reson Med 53:1347–1354, 2005. © 2005 Wiley-Liss, Inc.

Key words: diffusion; ADC; radial; projection reconstruction; MRI; stroke

Diffusion-weighted MRI (DWMRI) has become a powerful tool for investigating the translational motion of water within the human body. Because this motion is sensitive to the cellular architecture and integrity of the tissue, DWMRI has been used to investigate a number of diseases including stroke, cancer, and many other neurologic disorders (1–5). Many tissues, particularly in the brain, exhibit long-range structural order, which imparts anisotropy to the translational motion of water. This feature has been exploited in diffusion tensor imaging to investigate the integrity of white matter structures in the brain and to map out fiber orientations (6). In some applications, however, it is desirable to measure only the mean or average diffusivity, without the effects of anisotropy. This is the case in DWMRI of acute stroke where change in the apparent diffusion coefficient (ADC) of water is indicative of ischemic tissue. In such situations, anisotropy from organized structures can cause errors in calculations of ADC if diffusion is only measured in a single direction. To accu-

rately measure ADCs of water in anisotropic environments, a minimum of four individual DWMRI exams are typically carried out: one without diffusion weighting and three with diffusion weighting in orthogonal directions. The diffusion-weighted images can then be geometrically averaged to yield a “trace” image with average diffusion weighting (2). Because the trace of the diffusion tensor is invariant to rotation, the intensity in the resulting trace image is invariant to tissue orientation (7). A number of schemes for imparting isotropic diffusion weighting in individual DWMRI scans have been proposed (8). In the present paper we demonstrate a method that takes advantage of unique features of radial MRI data acquisition to achieve this purpose.

In radial MRI, Fourier data are collected along radial lines that all pass through the center of Fourier space. Each line, therefore, contributes more or less equally to the contrast in the final reconstructed image (9,10). If individual radial lines, or views, have different weightings, then images reconstructed from such data will have contrast determined by the average signal intensity from the different weightings. In radial fast spin-echo (radial-FSE) and radial gradient and spin-echo, for example, individual radial lines are collected at different TE times within spin echoes or gradient echoes and therefore have different T_2 and/or T_2^* weighting (11). While this variation can introduce artifacts in reconstructed images, it can also be exploited to produce multiple images with variable contrast from single radial data sets (11–13). In a diffusion-weighted radial-FSE sequence, this feature can be exploited to achieve effectively isotropic diffusion weighting within a single radial k -space data set, thereby increasing the imaging speed of multishot diffusion-weighted radial MRI.

In previous work, we have demonstrated a diffusion-weighted radial-FSE sequence for obtaining diffusion-weighted images with high spatial resolution and without significant artifacts due to motion and/or susceptibility (14–16). In this method, diffusion weighting is achieved in a preparation period where diffusion gradients are typically turned on in a constant direction while acquiring a full radial data set. This multishot method can yield higher spatial resolution than conventional single-shot techniques; however, it requires more imaging time. In the present work, we demonstrate a diffusion-weighted radial-FSE method for producing isotropic diffusion-weighted images from a single radial k -space data set by altering the direction of diffusion weighting gradients between TR periods. By selecting the appropriate diffusion weighting directions and view ordering, images can be generated that have effectively isotropic diffusion weighting without significant artifacts due to T_2 decay, motion, and/or diffusion anisotropy.

¹Biomedical Engineering Program, University of Arizona, Tucson, Arizona, USA.

²Department of Electrical and Computer Engineering, University of Arizona, Tucson, Arizona, USA.

³Department of Radiology, University of Arizona, Tucson, Arizona, USA.

⁴Optical Sciences Center, University of Arizona, Tucson, Arizona, USA.

Grant sponsor: National Institutes of Health; Grant number: R21 AG021624; Grant sponsor: Flinn Foundation.

*Correspondence to: Theodore P. Trouard, Biomedical Engineering Program, P.O. Box 245084, University of Arizona, Tucson, AZ 85724-5084, USA. E-mail: trouard@email.arizona.edu

Received 13 July 2004; revised 20 December 2004; accepted 29 December 2004.

DOI 10.1002/mrm.20493

Published online in Wiley InterScience (www.interscience.wiley.com).

© 2005 Wiley-Liss, Inc.

METHODS

An eddy current compensated diffusion-weighted radial-FSE sequence is shown in Fig. 1. The preparation period consists of CHESS presaturation of off-resonance fat, followed by a dual spin-echo (TE_1) in which eddy-current compensated diffusion gradients are played out (17). We have found that this preparation works well for suppressing artifacts due to eddy currents without sacrificing significant signal from the small increase in time needed to accommodate the second 180° RF pulse. Alternatively, simple Stejskal–Tanner diffusion weighting can be incorporated within a single spin echo preparation. Following this preparation, multiple views of Fourier data are acquired within a single TR period using a train of 180° RF refocusing pulses with an echo spacing of TE_2 . Within each data acquisition period, a full radial line is acquired by moving out to the end of a half radial line, collecting data while scanning back along a full radial line to the opposite side of k -space, and returning to the origin. The view ordering within the sequence is completely flexible for this trajectory and is chosen to minimize the effects of T_2 decay and motion artifacts (16). In general, the full 2π radians of Fourier space should be coarsely sampled within each echo train, i.e., each TR period, while differences in TE times for adjacent views are maximized. Artifacts due to motion are minimized by distributing motion errors about the full 2π radians of Fourier space instead of restricting them to sequential angular sections. This view ordering also reduces artifacts due to T_2 decay by spreading signal decay azimuthally with high angular frequency. The general expression for determining view angles, $\theta_{i,j}$, within an optimal view ordering is

$$\theta_{i,j} = [(i \cdot \Delta\theta_{\text{echo}} + m_i \cdot \Delta\theta) + j \cdot \text{ETL} \cdot \Delta\theta] \bmod \pi$$

where i is the echo index, j is the echo train index, echo train length (ETL) is the number of radial lines acquired each excitation, $\Delta\theta_{\text{echo}} = \pi/\text{ETL}$, and the angular separation between consecutive radial lines, $\Delta\theta = \pi/N$, where N is the total number of views collected. The $i \cdot \Delta\theta_{\text{echo}}$ term forces the full 2π radians of Fourier space to be coarsely sampled every TR period. The $m_i \cdot \Delta\theta$ term is responsible for mixing the TE times for adjacent views.

In isotropic diffusion-weighted radial-FSE, the diffusion weighting direction is varied during the acquisition of a

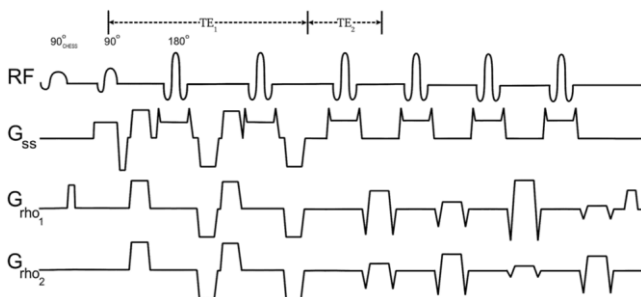


FIG. 1. Diagram of the isotropic diffusion-weighted radial-FSE pulse sequence with diffusion weighting in the XYZ direction and an ETL = 4.

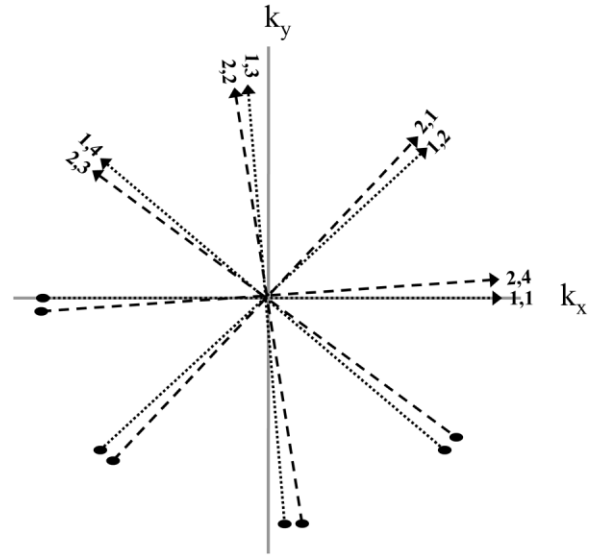


FIG. 2. View orientation for the first two TR periods of isotropic diffusion-weighted radial-FSE for a 256 view, ETL = 4 exam. The view labels are (echo train number, echo number).

full radial k -space data set such that images reconstructed from the data have effectively isotropic weighting. One practical approach steps through the set of directions $[1,1,1]$, $[-1,1,1]$, $[1,-1,1]$, $[-1,-1,1]$ (indicating full positive or negative gradient strength along the $[X, Y, Z]$ axes) during the scan. When arithmetically summed, this variation yields effectively isotropic weighting. By using full-strength gradients on each of the three gradient coils simultaneously, a desired diffusion weighting (b -value) can be obtained in the shortest amount of time (shortest TE). To reduce artifacts that could arise from anisotropic diffusion, adjacent views must be collected with different diffusion directions. Therefore, to reduce artifacts due to motion, T_2 decay, and diffusion anisotropy, view ordering must be carried out that (i) spreads radial lines acquired within a given TR period about the full 2π radians of Fourier space, (ii) maintains a high frequency variation of TE with view angle, (iii) maintains a high frequency variation of diffusion weighting direction with view angle, and (iv) does not correlate diffusion direction with TE. By using the view ordering described previously (16) and turning on diffusion weighting in each of the four directions for one-fourth the total TR periods consecutively, the data acquisition satisfies conditions i, ii, and iii. To satisfy condition iv, one more step had to be added to the view order calculation. After calculating the array of view angles, $\theta_{i,j}$, the views within a TR period undergo a circular left shift with respect to the echo index i . The view angles used in data acquisition $\theta_{i',j}$ are then defined by

$$\theta_{i',j} = \theta_{\text{CSL}(i, j \bmod \text{ETL}), j}$$

where $\text{CSL}(i,j)$ defines a circular shift to the left of index i by an amount $j \bmod \text{ETL}$. This view ordering results in the relationships described graphically in Figs. 2 and 3. In Fig. 2, the views obtained in the first two TR periods of a 256 view, ETL = 4 acquisition are shown. Within each TR

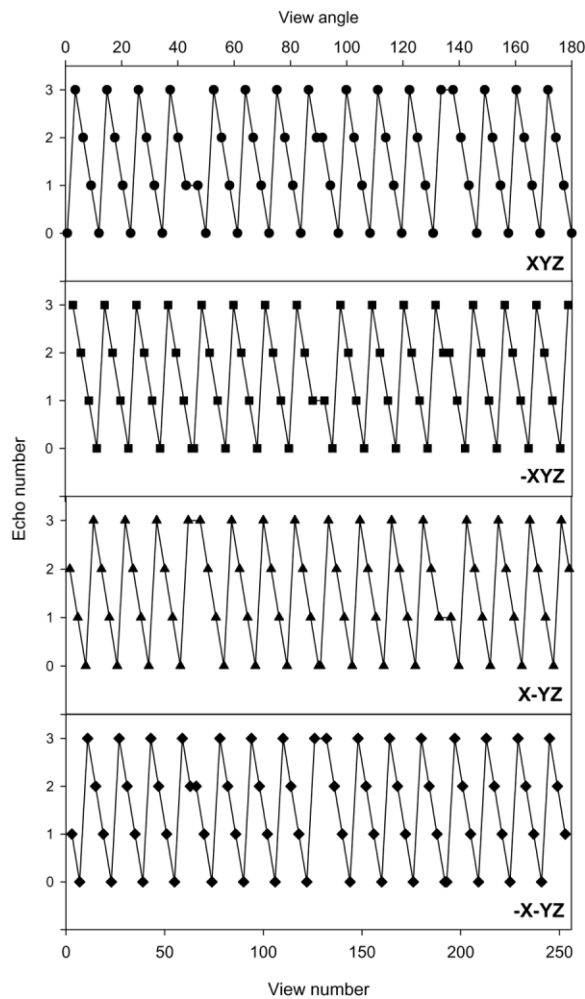


FIG. 3. Echo number versus view number for each of the four diffusion directions implemented in a 256 view, ETL = 4 isotropic diffusion-weighted radial-FSE exam. The diffusion weighting direction is given in each panel. Note the high frequency variation of both the echo position and the diffusion direction with view angle.

period, the entire range of view angles is coarsely sampled. The relationship among TE, diffusion weighting direction, and view angle is shown in Fig. 3. As can be seen, there is a high frequency variation of both TE and diffusion weighting direction with view angle and each diffusion weighting direction is collected at a variety of uncorrelated echo positions.

The isotropic diffusion-weighted radial-FSE sequence was implemented on GE Signa 1.5 T LX echospeed and GE Signa 3T MRI scanners (General Electric Medical Systems, Milwaukee, WI, USA) with actively shielded gradients capable of 33 and 40 mT/m, respectively. Image reconstruction of radial data sets was carried out offline using a magnitude filtered backprojection reconstruction (FBPR) implemented in IDL (Research Systems, Inc.) as described previously (18,19).

RESULTS

Diffusion-weighted images from the brain of healthy volunteers were obtained using the conventional and isotro-

pic diffusion-weighted radial-FSE methods. Representative images are shown in Fig. 4. Images collected with constant diffusion weighting in four individual directions within four individual exams are shown in Fig. 4a–d. The variation in signal intensity of white matter structures in the individual images indicates the anisotropic nature of the tissue. A trace image obtained from the geometric mean of these four images is shown in Fig. 4e and represents true isotropic diffusion weighting. An image of the same slice obtained with isotropic diffusion weighting in a single k -space data set is shown in Fig. 4f. Four identical isotropic scans were averaged to obtain an equivalent signal-to-noise ratio (SNR) for comparison to the trace image. The trace and isotropic diffusion-weighted radial-FSE images are qualitatively similar, indicating an effective averaging of anisotropic structures within the isotropic diffusion-weighted radial-FSE exam. The mean signal intensity from a region of interest (ROI) in the left splenium of the corpus callosum from each of the images in Fig. 4 is plotted in Fig. 5. While the signal intensity in 4 a–d varies significantly, the trace image and isotropic image have comparable mean signal intensity: 245.1 (\pm 23.9) and 250.8 (\pm 18.8) in the trace and isotropic images, respectively. Other anisotropic structures in the brain exhibit similar properties.

Conventional and isotropic diffusion-weighted radial-FSE was also carried out in patients undergoing DWMRI for acute stroke. Diffusion-weighted images of a stroke patient obtained using conventional and isotropic diffusion-weighted radial-FSE methods are shown in Fig. 6. Images obtained with constant diffusion weighting in four individual directions in four individual exams are shown in Fig. 6a–d. Figure 6e is the trace image produced from the geometric mean of these four images. The corresponding isotropic diffusion-weighted radial-FSE image is shown in Fig. 6f; this is from a single data set (no signal averaging) and thus it has approximately half the SNR of Fig. 6e, but required one-quarter of the time to acquire. The region of stroke can be clearly seen in both images without confounding hyperintensity from normal anisotropic white matter. The tissue affected by the stroke appears bright due to the reduced ADC associated with acute ischemia. The values of ADC in the region of the stroke obtained from ADC maps produced from the trace and isotropic images are 0.82×10^{-3} and 0.89×10^{-3} mm²/s, respectively. This can be compared to the ADC in normal white matter (1.28×10^{-3} and 1.31×10^{-3} mm²/s for the trace and isotropic exams, respectively), indicating a drop in ADC of approximately 34%, consistent with acute stroke. The isotropic radial-FSE method not only yields qualitatively equivalent images as the conventional method, but also quantitatively maintains all aspects of the areas of ischemia, regardless of the lower SNR.

DISCUSSION

A unique feature of all radial MRI methodologies is that the center of Fourier space is sampled by each radial line acquired. In the present paper, we have demonstrated that this feature enables high-resolution isotropic diffusion-weighted images to be obtained from a single radial k -space data set. While isotropic diffusion-weighted radial-

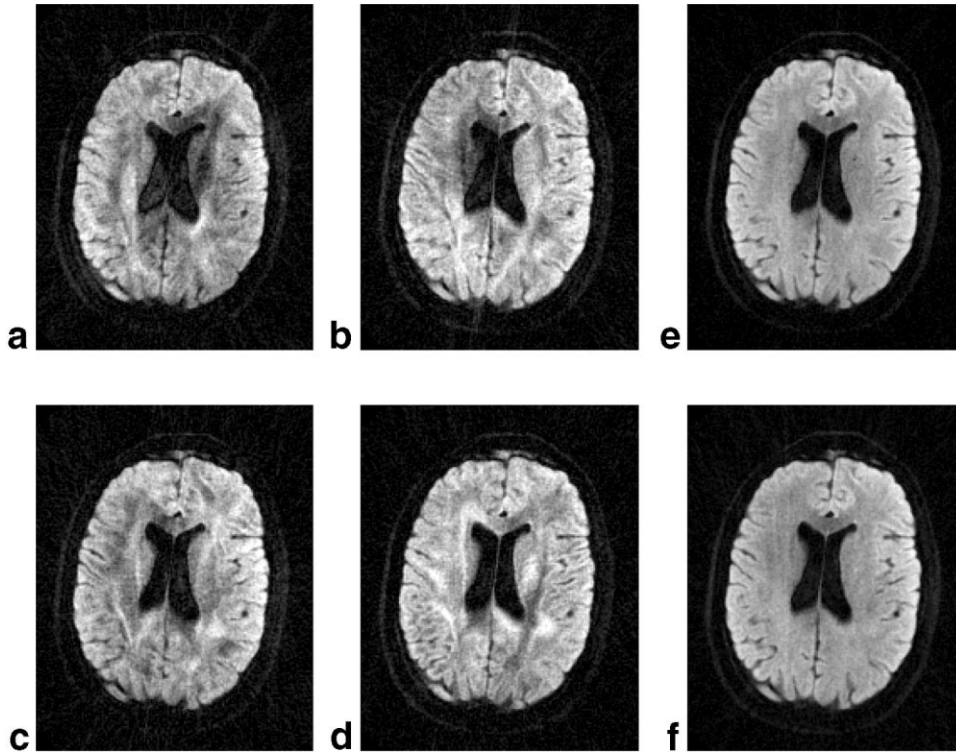


FIG. 4. Diffusion-weighted radial-FSE images of a normal volunteer at 1.5 T. Parameters for all images: $b = 1000 \text{ s/mm}^2$, $TE_1 = 70 \text{ ms}$, $TE_2 = 13 \text{ ms}$, $TR = 1500 \text{ ms}$, $ETL = 4$, $FOV = 26 \times 26 \text{ cm}^2$, with slice thickness = 5 mm. Images obtained with diffusion weighting in the XYZ, $-XYZ$, $X-YZ$, and $-X-YZ$ directions are shown in **a**, **b**, **c**, and **d**, respectively. A trace image produced from the geometric mean of these images is shown in **e**. An isotropic diffusion-weighted radial-FSE image is shown in **f**. This image was produced from the average of four identical exams so that signal to noise is comparable to that in **e**.

FSE produces images that have *effectively* isotropic diffusion weighting, they are not identical to true trace images produced from the average of individual data sets. When a trace image is produced from the geometric mean of n individual scans obtained with individual diffusion weighting, the resulting signal S_{trace} has the average diffusion weighting of the individual scans ($S_{1,2,\dots,n}$) and can be expressed as

$$\begin{aligned} S_{\text{trace}} &= \sqrt[n]{S_1 \times S_2 \dots \times S_n} \\ &= \sqrt[n]{S_0 e^{-bD_1} \times S_0 e^{-bD_2} \dots \times S_0 e^{-bD_n}} \end{aligned}$$

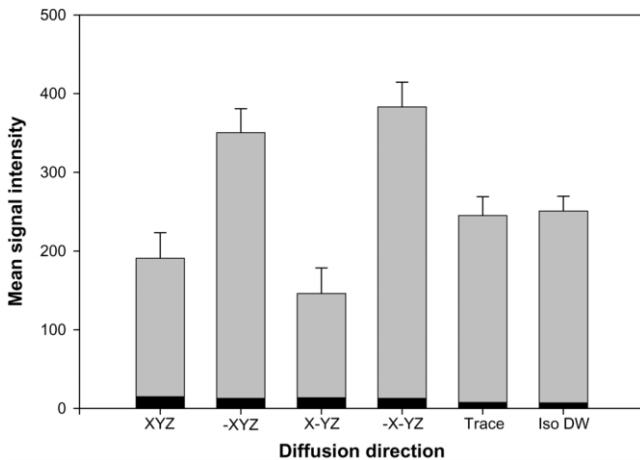


FIG. 5. The mean signal intensity for identical ROIs in the left splenium of the corpus callosum from images in Fig. 4; the black bar indicates the noise level in each image.

$$= S_0 \sqrt[n]{e^{-b(D_1 + D_2 \dots + D_n)}} = S_0 \sqrt[n]{e^{-nbD_{\text{ave}}}} = S_0 e^{-bD_{\text{ave}}},$$

where it is assumed that k appropriate diffusion directions were selected such that

$$D_{\text{ave}} = \frac{1}{n} \sum_{k=1}^n D_k.$$

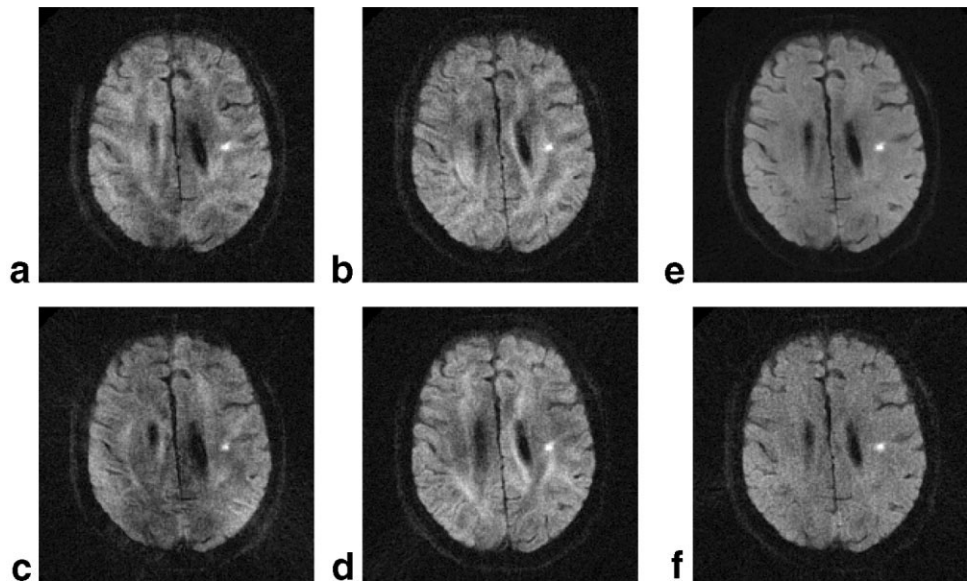
The FBPR process used in reconstruction of radial data sets, however, is a linear operation and results in an arithmetic averaging of the signal obtained from the set of diffusion directions chosen. Additionally, there is an individual point-spread function (PSF) associated with the angular undersampling of each diffusion direction. The signal in an isotropic diffusion-weighted radial-FSE image, S_{iso} , can be written as

$$\begin{aligned} S_{\text{iso}} &= \frac{S_1 + S_2 \dots + S_n}{n} \\ &= \frac{S_0 e^{-bD_1} * \text{psf}_1 + S_0 e^{-bD_2} * \text{psf}_2 \dots + S_0 e^{-bD_n} * \text{psf}_n}{n} \\ &= \frac{S_0}{n} (e^{-bD_1} * \text{psf}_1 + e^{-bD_2} * \text{psf}_2 \dots + e^{-bD_n} * \text{psf}_n). \end{aligned}$$

If diffusion in the tissue is isotropic, then $D_1 = D_2 = D_n = D_{\text{ave}}$ and $\text{psf}_1 + \text{psf}_2 \dots + \text{psf}_n = \delta$ (delta function), leaving

$$S_{\text{iso}} = \frac{S_0}{n} (n e^{-bD_{\text{ave}}}) = S_0 e^{-bD_{\text{ave}}}.$$

FIG. 6. Diffusion-weighted radial-FSE images of a stroke patient acquired at 1.5 T. Parameters for all images: $b = 1000$ s/mm², $TE_1 = 70$ ms, $TE_2 = 13$ ms, $TR = 1000$ ms, $ETL = 4$, $FOV = 26 \times 26$ cm², with slice thickness = 5 mm. Images obtained with diffusion weighting in the XYZ, -XYZ, X-YZ, and -X-YZ directions are shown in a, b, c, and d, respectively. A trace image produced from the geometric mean of these images is shown in e. The corresponding isotropic diffusion-weighted radial-FSE image is shown in f.



If the tissue is anisotropic, however, the true average diffusion-weighted signal will be multiplied by a small factor, which is always positive, making the signal in the isotropic diffusion-weighted radial-FSE image slightly higher than that of the trace image. This relationship is shown graphically in Fig. 7. Calculated signal intensity from three diffusion-weighted data sets, with a b -value = 1000 s/mm², using arithmetic (dashed line) and geometric (solid line) averaging, are plotted versus fractional anisotropy (FA). The mean diffusivity was chosen to be 1.0×10^{-3} mm²/s to represent white matter. The relationship between the diffusion coefficient for the three orthogonal directions range from equal values (FA = 0) to diffusion in only one direction (FA = 1.0). The error produced from the

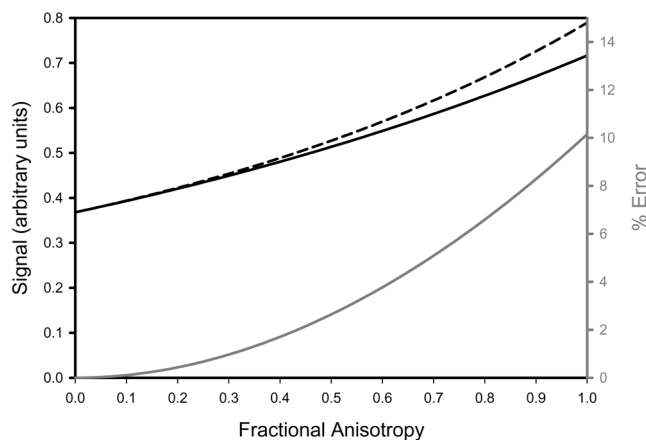


FIG. 7. Signal intensity versus fractional anisotropy expected from three orthogonal diffusion-weighted data sets using arithmetic (black dashed line) or geometric (black solid line) averaging. The data were produced assuming $b = 1000$ s/mm² and mean diffusivity of 1.0×10^{-3} mm²/s. The relationship between the diffusion coefficients for the three orthogonal directions ranges from equal values (FA = 0) to diffusion in only one direction (FA = 1.0). The error produced from the arithmetic averaging is shown as a percentage of the geometric mean (gray solid line).

arithmetic averaging is shown in Fig. 7 as a percentage of the geometric mean. For isotropic structures, the two calculations are identical. At FA = 0.8, an appropriate value for highly anisotropic white matter, the error is approximately 6.6%. Such small error is consistent with the experimental results shown in Figs. 4 and 5.

Due to the motion insensitivity of radial MRI, reconstructed radial-FSE images are free from significant motion artifacts and due to the fast spin-echo refocusing utilized in the sequence, images have no susceptibility artifacts as in conventional DWMRI methodology. Figure 8a is a diffusion-weighted trace image obtained with single-shot echo planar imaging (SSEPI). Three images obtained with diffusion weighting in three orthogonal directions were averaged to obtain the trace image. An isotropic diffusion-weighted radial-FSE image of the same patient is shown in Fig. 8b. In both images, areas of ischemia are clearly visible as regions of hyperintensity, there is no obscuring bright signal due to diffusion anisotropy in white matter, and there are no artifacts due to motion. However, the lower resolution SSEPI method is unable to resolve the two smaller anterior areas of ischemia, seen in the higher resolution radial-FSE image. The lack of image distortion in the radial-FSE image also allows for a more direct comparison of diffusion-weighted images to conventional T_2 -weighted and T_1 -weighted images. Similar results have been obtained consistently in our clinical evaluations.

Because radial-FSE is insensitive to magnetic field inhomogeneity, it works well at higher field strengths. A comparison of isotropic diffusion-weighted radial-FSE with SSEPI at 3 T is shown in Fig. 9. These images are from a patient with a renal cell carcinoma metastasis within the right hemisphere and were obtained after the injection of a contrast agent, Omniscan, which has been shown to have insignificant effects on DWMRI (20). DWMRI is being used to evaluate the cellularity of cancerous tissues (21) and to predict tumor response to chemotherapy (3,22–24). The SSEPI images in Fig. 9 have 3.75×3.75 mm² in plane resolution and show typical susceptibility artifacts in the frontal and temporal lobe regions due to air-tissue inter-

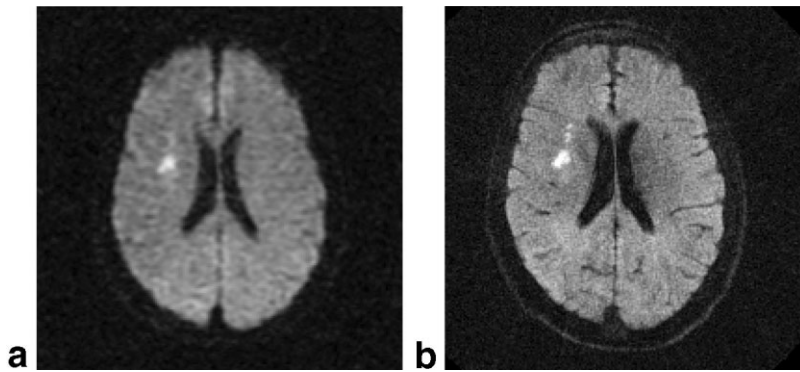


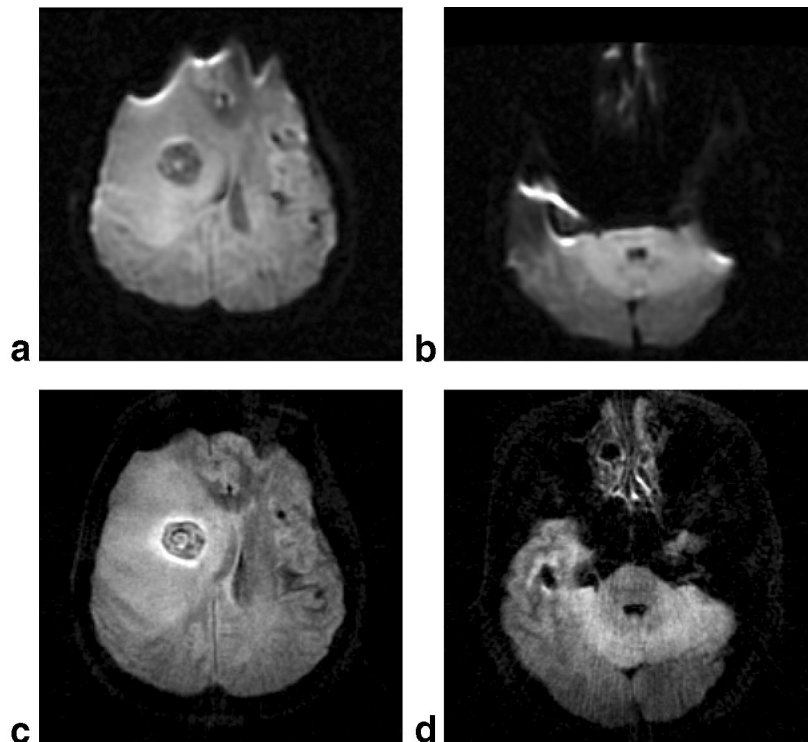
FIG. 8. Diffusion-weighted images acquired on the 1.5 T scanner of a stroke patient ($b = 1000 \text{ s/mm}^2$) using SSEPI (a) and isotropic diffusion-weighted radial-FSE (b). For the SSEPI exam $TE = 81 \text{ ms}$, $TR = 10 \text{ s}$, $FOV = 30 \times 20 \text{ cm}^2$, with slice thickness = 5 mm. For the radial-FSE exam, $TE_1 = 70 \text{ ms}$, $TE_2 = 13 \text{ ms}$, $TR = 1500 \text{ ms}$, $ETL = 4$, $FOV = 26 \times 26 \text{ cm}^2$, with slice thickness = 5 mm.

faces. No detail is visible within or adjacent to the tumor. The isotropic diffusion-weighted radial-FSE images shown in Fig. 9c and d have $0.94 \times 0.94 \text{ mm}^2$ in-plane resolution and are free of motion and susceptibility artifacts. Due to the high resolution of the radial-FSE images and insensitivity to susceptibility changes, heterogeneity within and around the tumor can be clearly visualized (Fig. 9c). Because this metastasis was hemorrhagic, it contains blood products that yield regions of local susceptibility gradients that cause problems for SSEPI methods.

A unique feature of isotropic diffusion-weighted radial-FSE is that both ADC maps and T_2 maps can be generated from only two data sets. A high-resolution ADC map, obtained from two individual exams ($b = 5 \text{ s/mm}^2$ and $b = 1000 \text{ s/mm}^2$ in Fig. 10a and b, respectively) is shown in Fig. 10c. ADC values in the brain unaffected by the stroke are similar to those given in literature (1.17×10^{-3} and $1.32 \times 10^{-3} \text{ mm}^2/\text{s}$ for white matter and gray matter, respectively) and there is a decrease in the ADC in the region of ischemia ($0.72 \times 10^{-3} \text{ mm}^2/\text{s}$ versus 0.96×10^{-3}

mm^2/s in homologous tissue on the contralateral side) (25,26). It is important to note that measured ADC values are dependent on the amount of diffusion weighting applied, the diffusion time, and the TE of the sequence (26). ADC values in regions of ischemia are also dependent on the time elapsed between stroke onset and the DWMRI exam. Maps of T_2 can be calculated from any individual isotropic radial-FSE data set. An example of this is shown in Fig. 10d where a T_2 map was generated from the non-diffusion-weighted ($b = 5 \text{ s/mm}^2$) isotropic radial-FSE data set (Fig. 10a), with a postprocessing technique described previously (12,13). Briefly, multiple images at different effective TE values are produced from one radial-FSE data set. For reconstruction of an image at a particular effective TE, only views acquired at that TE provide data near the center of k -space (within the Nyquist radius). At higher spatial frequencies, data from views with other TEs are included (13). A T_2 map is then calculated from the TE images using a single exponential decay fit. There is an increase of T_2 in the region of ischemia (139.8 ms versus

FIG. 9. Diffusion-weighted images ($b = 1000 \text{ s/mm}^2$) of a cancer patient acquired at 3 T using SSEPI (a,b) and isotropic diffusion-weighted radial-FSE (c,d). Imaging parameters for the SSEPI exam were $TE = 72 \text{ ms}$, $TR = 10 \text{ s}$, $FOV = 30 \times 20 \text{ cm}^2$, and slice thickness = 5 mm. Imaging parameters for the radial-FSE exam were $TE_1 = 60 \text{ ms}$, $TE_2 = 15 \text{ ms}$, $TR = 3000 \text{ ms}$, $ETL = 4$, $FOV = 26 \times 26 \text{ cm}^2$, with slice thickness = 5 mm.



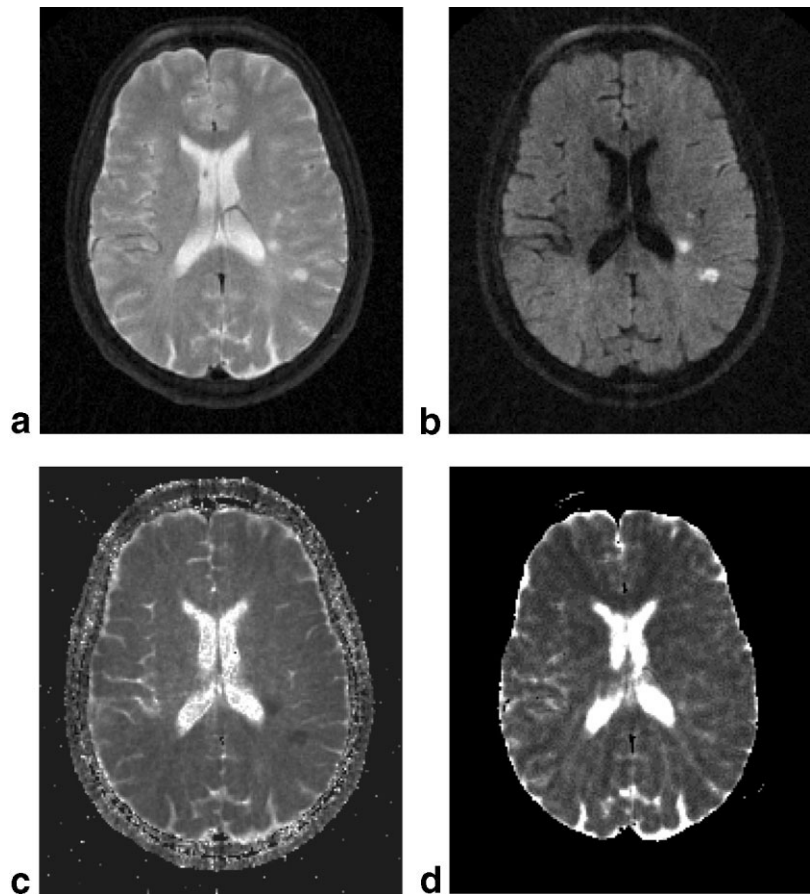


FIG. 10. Images acquired on the 1.5 T scanner of a stroke patient using isotropic diffusion-weighted radial-FSE. For all images $TE_1 = 70$ ms, $TE_2 = 13$ ms, $TR = 1500$ ms, $ETL = 4$, $FOV = 26 \times 26$ cm², slice thickness = 5 mm. (a) is the $b = 5$ s/mm² image, and (b) is the $b = 1000$ s/mm² image. An ADC map calculated from the radial-FSE data set is shown in (c). A T_2 map calculated from the radial-FSE $b = 5$ s/mm² image is shown in (d).

110.2 ms in the contralateral side). This region of ischemia shows a decreased ADC with an elevated T_2 , consistent with acute stroke imaged between 6 and 48 hr (1,27). The ability to quantitatively determine both ADC and T_2 in ischemic tissue may help determine the age of the stroke, which plays an important role in therapeutic decisions (28).

Other methods have been developed to obtain effectively isotropic diffusion weighting within the preparation period of a sequence (8). A common feature of these methods is that they require an increased amount of time to achieve a given diffusion weighting (compared to Stejskal-Tanner type weighting). Because the diffusion-preparation periods are then required to be longer, the minimum TE time increases, resulting in a loss of SNR. Also, it is not always possible to make such sequences eddy current compensated, which we have found to be very helpful in both radial and Cartesian DWMRI. Because subsets of the radial data are acquired with diffusion weighting in different directions, it may be possible to obtain information on diffusion anisotropy within a single radial data set (29). This is similar to producing T_2 maps from individual radial-FSE data sets as described previously (12,13) and is currently being investigated.

CONCLUSIONS

The present paper demonstrates a simple method for obtaining isotropic diffusion weighting in a single radial MRI

exam. Using the appropriate view ordering and diffusion weighting, radial-FSE images can be acquired with high spatial resolution that are insensitive to bulk motion, susceptibility changes, T_2 decay, and diffusion anisotropy. Radial-FSE also allows for T_2 maps to be generated from individual exams such that both ADC and T_2 maps can be obtained from only two radial-FSE exams.

REFERENCES

1. Warach S, Gaa J, Siewert B, Wielopolski P, Edelman RR. Acute human stroke studied by whole brain echo planar diffusion-weighted magnetic resonance imaging. *Ann Neurol* 1995;37:231–241.
2. van Gelderen P, de Vleeschouwer M, DesPres D, Pekar J, van Zijl P, Moonen C. Water diffusion and acute stroke. *Magn Reson Med* 1994; 31:154–163.
3. Chenevert TL, McKeever PE, Ross BD. Monitoring early response of experimental brain tumors to therapy using diffusion magnetic resonance imaging. *Clin Cancer Res* 1997;3:1457–1466.
4. Nakahara M, Ericson K, Bellander BM. Diffusion-weighted MR and apparent diffusion coefficient in the evaluation of severe brain injury. *Acta Radiol* 2001;42:365–369.
5. Bammer R, Fazekas F. Diffusion imaging in multiple sclerosis. *Neuroimaging Clin North Am* 2002;12:71–106.
6. Pierpaoli C, Basser PJ. Toward a quantitative assessment of diffusion anisotropy. *Magn Reson Med* 1996;36:893–906.
7. Basser PJ, Mattiello J, Le Bihan D. MR diffusion tensor spectroscopy and imaging. *Biophys J* 1994;66:259–267.
8. Wong E, Cox R, Song A. Optimized isotropic diffusion weighting. *Magn Reson Med* 1995;34:139–143.
9. Hall LD, Sukumar S. Rapid data-acquisition for NMR imaging by projection-reconstruction method. *J Magn Reson* 1984;56:179–182.

10. Rasche V, Holz D, Schepper W. Radial turbo spin echo imaging. *Magn Reson Med* 1994;2:629–638.
11. Gmitro AF, Kono M, Theilmann RJ, Altbach MI, Li Z, Trouard TP. Radial GRASE: Implementation and Applications. *Magn Reson Med* 2005;53:1363–1371.
12. Song HK, Dougherty L. k-Space weighted image contrast (KWIC) for contrast manipulation in projection reconstruction MRI. *Magn Reson Med* 2000;44:825–832.
13. Altbach MI, Outwater EK, Trouard TP, Krupinski EA, Theilmann RJ, Stopeck AT, Kono M, Gmitro AF. Radial fast spin-echo method for T2-weighted imaging and T2 mapping of the liver. *J Magn Reson Imaging* 2002;16:179–189.
14. Trouard TP, Theilmann RJ, Altbach MI, Gmitro AF. High-resolution diffusion imaging with DIFRAD-FSE (diffusion-weighted radial acquisition of data with fast spin-echo) MRI. *Magn Reson Med* 1999;42:11–18.
15. Trouard TP, Saul J, Seeger J, Theilmann RJ, Altbach MI, Gabaeff D, Gmitro AF. Comparison of DIFRAD-FSE with single-shot EPI for diffusion-weighted MRI of acute stroke. In: Proceedings of the 10th Annual Meeting of ISMRM, Honolulu, 2002. p 1114.
16. Theilmann RJ, Gmitro AF, Altbach MI, Trouard TP. View-ordering in radial fast spin-echo imaging. *Magn Reson Med* 2004;51:768–774.
17. Reese TG, Heid O, Weisskoff RM, Wedeen. Reduction of eddy-current-induced distortion in diffusion MRI using a twice-refocused spin echo. *Magn Reson Med* 2003;49:177–182.
18. Gmitro AF, Alexander AL. Use of projection reconstruction imaging method to decrease motion sensitivity in diffusion-weighted MRI. *Magn Reson Med* 1993;29:835–838.
19. Jung K, Cho ZH. Reduction of flow artifacts in NMR diffusion imaging using view-angle tilted line-integral projection reconstruction. *Magn Reson Med* 1991;19:249–293.
20. Yamada K, Kubota H, Kizu O, Nakamura H, Ito H, Yuen S, Tanaka O, Kubota T, Makino M, Van Cauteren M, Nishimura T. Effect of intravenous Gadolinium-DTPA on diffusion-weighted images, evaluation of normal brain and infarcts. *Stroke* 2002;33:1799–1802.
21. Sugahara T, Korogi Y, Kochi M, Ikushima I, Shigematu Y, Hirai T, Okuda T, Liang L, Ge Y, Komohara Y, Ushio Y, Takahashi M. Usefulness of diffusion-weighted MRI with echo-planar technique in the evaluation of cellularity in gliomas. *J Magn Reson* 1999;9:53–60.
22. Galons JP, Altbach MI, Paine-Murrieta GD, Taylor CW, Gillies RJ. Early increases in breast tumor xenograft water mobility in response to Paclitaxel therapy detected by non-invasive diffusion magnetic resonance imaging. *Neoplasia* 1999;1:113–117.
23. Zhao M, Pipe JG, Bonnett J, Evelhoch JL. Early detection of treatment response by diffusion-weighted H-NMR spectroscopy in a murine tumour in vivo. *Br J Cancer* 1996;73:61–64.
24. Jennings D, Hatton BN, Guo J, Galons JP, Trouard TP, Raghunand N, Marshall J, Gillies RJ. Early response of prostate carcinoma xenografts to docetaxel chemotherapy monitored with diffuson MRI. *Neoplasia* 2002;4:255–262.
25. Sorensen AG, Buonano FS, Gonzalez RG, Schwamm LH, Lev MH, Huang-Hellinger FRH, Reese TG, Weisskoff RM, Davis TL, Suwanwela N, Can U, Moreira JA, Copen WA, Look RB, Finklestein SP, Rosen BR, Koroshetz WJ. Hyperacute stroke: evaluation with combined multislice diffusion-weighted and hemodynamically weighted echo-planar MR imaging. *Radiology* 1996;199:391–401.
26. Yoshiura T, Wu O, Zaheer A, Reese TG, Sorensen AG. Highly diffusion-sensitized MRI of brain: Dissociation of gray and white matter. *Magn Reson Med* 2001;45:734–740.
27. Welch KMA, Windham J, Knight RA, Nagesh V, Hugg JW, Jacobs M, Peck D, Booker P, Dereski MO, Levine SR. A model to predict the histopathology of human stroke using diffusion and T2-weighted magnetic resonance imaging. *Stroke* 1995;26:1983–1989.
28. Eastwood JD, Engelter ST, MacFall JF, Delong DM, Provenzale JM. Quantitative assessment of the time course of infarct signal intensity on diffusion-weighted images. *Am J Neuroradiol* 2003;24:680–687.
29. Newbould RD, Sarlls JE, Trouard TP. Data collection and post-processing strategies in radial-FSE for diffusion tensor analysis. In: Proceedings of the 12th Annual Meeting of ISMRM, Kyoto, Japan, 2004. p 446.